NATIONAL ADVISORY COMMITTEE FOR AERONAUTICS

TECHNICAL MEMORANDUM

No. 1157

* 8 DEC 1947

CONES IN SUPERSONIC FLOW

By W. Hantzsche and H. Wendt

Translation

"Mit Überschallgeschwindigkeit angeblasene Kegelspitzen"

Jahrbuch 1942 der deutschen Luftfahrtforschung, pp. I 80-I 90

Washington
August 1947

N A C A LIBRARY
LANGLEY MEMORIAL AERONAUTICAL
LABORATORY
Langley Field, Va.

NASA Technical Library
3 1176 01437 4616

NATIONAL ADVISORY COMMITTEE FOR AERONAUTICS

TECHNICAL MEMORANDUM NO. 1157

CONICAL TIPS IN SUPERSONIC FLOW*

By W. Hantzsche and H. Wendt

In the case of cones in axially symmetric flow of supersonic velocity, adiabatic compression takes place between shock wave and surface of the cone. Interpolation curves between shock polars and the surface are therefore necessary for the complete understanding of this type of flow. They are given in the present report by graphical-numerical integration of the differential equation for all cone angles and airspeeds.

INTRODUCTION

The assumption that a velocity potential exists in gas flows with supersonic velocity is complied with in few specific cases only. The expansion of a gas around a corner (reference 1), a closed integrable example of a supersonic flow, and the flow against a wedge are common knowledge. It is true that a compressibility shock occurs on the latter, but the flow after the shock is a parallel flow again, at least in the cases where the shock begins at the tip of the wedge. In 1929 Busemann (reference 2) discussed the case of conical tips in axial flow. In this instance, when the cone angle for fixed Mach number is not too great, the flow after the shock is the simplest case of a more general type, the so-called conical fields, subsequently discussed in greater detail by Busemann (reference 3). These are (not necessarily rotation free) dimensionless flows which are reflected on themselves by similar distortion from a certain point. All straight lines through the center of similarity are carriers of equal states of gas (speed, pressure, density). The axial conical field following a parallel flow occurs, aside for flow against conical tips, also for a certain type of compression nozzle.

The present report is intimately linked to Busemann's axial conical fields, but deals only with cones. The exact data and the further interpretation of Busemann's apple curves (Apfelkurven) are given.

---

*"Mit Überschallgeschwindigkeit angeblasene Kegelspitzen," Jahrbuch 1942 der deutschen Luftfahrtforschung, pp. I80 - I90.

THE WEDGE IN SUPERSONIC FLOW

If a compressibility shock occurs in a two-dimensional stationary gas flow, the following equations from the continuity, the momentum balance, and the energy law are applicable:

$$\rho_1 w_{1n} = \rho_2 w_{2n} \tag{1}$$

$$p_1 + \rho_1 w_{1n}^2 = p_2 + \rho_2 w_{2n}^2 \tag{2a}$$

$$\rho_1 w_{1n} w_{1t} = \rho_2 w_{2n} w_{2t} \tag{2b}$$

$$i_1 + \frac{1}{2} w_1^2 = i_2 + \frac{1}{2} w_2^2 \tag{3}$$

Subscripts:

1 quantities before shock

2 quantities after shock

Quantities w_n and w_t are the velocity components normal and parallel to the shock surface, ρ the density, p the pressure, and i the heat content (fig. 1). Equation (2b), together with equation (1), indicates that $w_{t1} = w_{t2}$, hence, that the tangential component of the velocity remains unchanged at the shock.

The shock process is preferably followed in hodographs with cartesian coordinates u, v. The states (u_2, v_2) obtainable by shock from a certain initial speed located, say in the u-axis (u_1), lie on the closed branch of a cartesian sheet of the shock polars, (fig. 2) whose equation for an ideal gas is readily derived from equations (1) to (3):

$$v_2 = (u_1 - u_2)\sqrt{\frac{u_2 - \frac{a^{*2}}{u_1}}{\frac{a^{*2}}{u_1} + \frac{2}{\kappa + 1} u_1 - u_2}} \tag{4}$$

a^* is the critical velocity, $\kappa = \frac{c_p}{c_v}$ the ratio of the specific heats at constant pressure and volume. The normal on the length

connecting the state before and after the shock, a chord, obviously indicates the direction of the shock surface with respect to the flow, because at the shock only the normal component is subjected to a discontinuity. Thus the flow against a wedge with the angle 2δ in figure 3 corresponds to the conditions represented in figure 2. The limiting value toward which the angle tends at decreasing intensity of compressibility shock is, therefore, the Mach angle. The upper limit for γ is 90° and appears with a straight compressibility shock $\left(u_2 = \frac{a^{*2}}{u_1} v_2 = 0\right)$. Figure 2 also shows for fixed Mach number a maximum deflection, that is, a greatest possible wedge angle. For wedges with smaller angle two compressibility shocks are possible, one of which generally leads to supersonics and one to subsonics. The practically occurring solution, denoted as stable, is the supersonic solution, which, as demonstrated by G. Guderley can also be proved experimentally. Since the contact point of the tangent from the zero point of the hodograph to the shock polar does not, in general, coincide with the intersection point A of the circle of the critical velocity, but still lies in the subsonic zone, there are two subsonic solutions for wedge angles on the, admittedly, very small arc between A and B.

For a wedge in a flow at angle greater than the maximum a curved shock area before the wedge results. The flow after the shock is no longer potential flow, the entropy jump along each streamline is different (fig. 4). All points of the shock polar are realized. Far from the wedge the compressibility shock runs out in a Mach wave; this corresponds to the supersonic end of the shock polars. On the line of symmetry before the wedge is a straight compressibility shock, that is, the subsonic end of the polars. Between the two states lie in steady sequence the other points, particularly point A of the critical velocity and point B of the maximum deflection. On the subject of separation of the shock area from the tip, L. Crocco (reference 4) established, in an exact theoretical analysis of slightly curved wedge surfaces, that this separation must take place before reaching the maximum angle, which is, to be exact, for a point of the shock polars between A and B. One essential condition being, of course, that the curvature at the wedge edge is other than zero. On considering Crocco's critical point on the shock area separated from the body, the streamline there can start only with the curvature zero.

Lastly, the variation of the pressure difference $p_2 - p_1$ referred to dynamic pressure $\frac{1}{2}\rho_1 u_1^2$ and the ratio $\frac{p_o'}{p_o}$ of

the tank pressure before and after the shock follows as

$$\frac{p_2 - p_1}{\frac{1}{2}\rho_1 u_1^2} = 2\left(1 - \frac{u_2}{u_1}\right) \tag{5}$$

$$\frac{p_o'}{p_o} = \left[\frac{(\kappa + 1)\tan(\gamma - \delta) - (\kappa - 1)\tan\gamma}{(\kappa + 1)\tan\gamma - (\kappa - 1)\tan(\gamma - \delta)}\right]^{\frac{1}{\kappa-1}} \left[\frac{\tan\gamma}{\tan(\gamma - \delta)}\right]^{\frac{\kappa}{\kappa-1}} \tag{6}$$

with equation (6) the entropy jump

$$\Delta s = R \ln \frac{p_o}{p_o'} \qquad (R = \text{gas constant})$$

is known.

THE CONE IN SUPERSONIC FLOW

For a solid of rotation in straight flow, when the shock surface adheres to the cone tip, the flow after the shock is a conical field. The shock surface is a coaxial cone of rotation (fig. 5). The compressibility shock on the entire cone envelope has the same strength. In all points of each straight line through the cone origin the velocity is constant in magnitude and direction; the state of gas, the same. The shock conditions (1) to (2) are exactly the same as for two-dimensional flow, when, as before, w_t and w_n denote the velocity components parallel and at right angles to the shock area. (Owing to the axial symmetry, w_t and w_n lie in an axial section of the cone.) Their erection merely requires the plane tangential element to the shock area. The potential flow following the shock is naturally no longer a parallel flow in the axial section - it would be incompatible with the continuity condition - the streamlines rather become asymptotically narrower (fig. 6). Figure 7 shows the conditions in the hodograph for one axial section, with u and v denoting the velocity components parallel and at right angles to the axis of rotation. Because of the conical character of the flow in the hodograph all streamlines are represented by the same curve. The velocity before the shock is along the axis of the abscissa (u_1). At the shock cone with the cone angle 2γ the streamlines are deflected by the angle δ,

as seen from the shock polar related to u_1. The new state u_2, v_2 is transferred by adiabatic compression to the state u_3, v_3 at the cone envelope. Angle β is then half the included angle of the cone. A closer examination of the conical field indicates (compare references 2 and 3) that the normal in a certain point P' of the meridian curve runs parallel to the straight line through the cone tip, which carries the gas state defined by P', as exemplified in figures 6 and 7 for the state u', v' with the normal of the slope ϕ'. For the end point u_3, v_3 direction of velocity and slope of the normal are coincident. Owing to this arrangement of streamline and meridian line, the specification of a meridian line characterizes a cone in axial flow. To obtain a survey over all conical flows, either the cone opening angle at the same airspeed, hence the shock polars, or, which is the same, the strength of the compressibility shock can be varied (fig. 8). The locus of the thus obtainable states on the cone envelope, the connecting line of the end points of the individual meridian curves, is called "apple curve" because of its particular shape. Furthermore, the airspeed can be varied, so that to each shock polar or each Mach number of flow there corresponds a different apple curve.

The conical field after the compressibility shock has a potential and is (u and v again denoting the velocity components in the axial section parallel and at right angles to the axis) characterized by the differential equation

$$vv'' = 1 + v'^2 - \frac{(u + vv')^2}{a^2} \tag{7}$$

The dashes indicate derivations with respect to u; a^2 signifies the square of the local sonic velocity which for ideal gases is linked with the speed by the relation

$$a^2 = \frac{\kappa + 1}{2}a^{*2} - \frac{\kappa - 1}{2}(u^2 + v^2) \tag{8}$$

The meridian curves are integral curves of equation (7) with the boundary condition (fig. 7) in the point u_2, v_2 of the shock polars with the slope of the connecting line from $(u_1, 0)$ toward (u_2, v_2). This means that the potential flow must precede the state of gas produced by the compressibility shock. Moreover, since the normal to the meridian curve indicates the polar angles of the respective state, the condition for the initial slope is necessary for reasons

of continuity. The end of the meridian line is given by the requirement that the normal pass through the zero point of the hodograph: $u + vv' = 0$. Direction of velocity and of normal must be identical.

For the practical determination of the meridian curve, a graphical method based on the shape (identical with equation (7)) of its different equation

$$R = -\frac{N}{1 - \frac{U^2}{a^2}} \tag{9}$$

is appropriate. Here (fig. 9) R is the radius of curvature, N the normal section between meridian curve and U-axis, and U the length of the perpendicular $U = \frac{u + vv'}{\sqrt{1 + v'^2}}$ from the zero point of the hodograph to the normal. As α is a function of the velocity (formula (8)), the curvature radius R in a point of the meridian curve can be computed by marking off U, N, and $w = \sqrt{u^2 + v^2}$. In the practical performance of this progressive construction it is found that the meridian lines are, in general, obtained fairly accurately. This was checked by integration of equation (7) by the Runge-Kutta approximation process for ordinary differential equations. A departure in graphical accuracy occurs only at the meridian curves arising near the ends of the shock polars, that is near the axis. Most easily uncertain in the graphical determination is the position of the end point u_3, v_3 on the meridian curve, and with it the cone angle. In order to obtain it also relatively exact, individual meridian lines were mathematically checked at points where their variation had been satisfactorily represented by the construction. The applicability even of the Runge-Kutta method to the meridian curves near the axis is limited. But here equation (7) affords approximations where the last term at the right is taken equal to the constant initial value $\frac{u_1^2}{a_1^2}$ in the neighborhood of $(u_1, 0)$ and $\frac{\bar{u}_1^2}{\bar{a}_1^2}$ in the vicinity of $\left(\bar{u}_1 = \frac{a^2}{u_1}, 0\right)$. Quantities a_1 and $\bar{a}_1$ are the sonic velocities related to $(u_1, 0)$ and $(\bar{u}_1, 0)$.

The shape of the meridian curves is then:

$$v = A\sqrt{\frac{u_1^2}{a_1^2} - 1}\,\sin\frac{u_1 - u}{A} \text{ supersonic} \tag{10a}$$

$$v = v_2 \cos\frac{\bar{u}_1 - u}{v_2}\sqrt{1 - \frac{\bar{u}_1^2}{\bar{a}_1^2}} \text{ subsonic} \tag{10b}$$

The marked approximation character of these formulas is readily apparent from the fact that in equation (10a) for all values of the parameter A the curves pass through the point $u = u_1, v = 0$, have the same initial shape $\sqrt{\frac{u_1^2}{a_1^2} - 1}$ and the initial curvature zero. In equation (10b) the curves pass through the initial points $(\bar{u}_1, v_2)$ but have the same initial zero slope. In spite of that, the approximations are sufficient to reproduce the behavior of the apple curves near the "blossom" and the "stem," where a logarithmic singularity occurs:

$$u_3 = u_1 - \frac{v_3^2}{u_1}\ln - \frac{2}{\sqrt{\frac{u_1^2}{a_1^2} - 1}}\frac{u_1}{v_3} \text{ supersonic} \tag{11a}$$

$$u_3 = \bar{u}_1 - \frac{v_3^2}{\bar{u}_1}\ln\frac{2}{\sqrt{1 - \frac{\bar{u}_1^2}{a_1^2}}}\frac{\bar{u}_1}{v_3} \text{ subsonic} \tag{11b}$$

On comparing the graphical integration for the different shock polars it is found to be best for the maximum velocities. For the higher Mach numbers the curvature radii are too great to ensure good construction. However, this is usually overcome by substituting straight lines for the arcs. But for Mach numbers near unity, on the other hand, the construction becomes very inaccurate because of the abnormal curvature variation along the meridian line. For the vicinity of the critical velocity there is an approximation by Busemann which, however, does not become accurate except at very small shock polars as will be discussed later.

The airspeeds employed for the graphical numerical integration of equations (7) and (9) correspond to the pressure factors (999.9915), 996, 992, 988, . . . 964, 956, 945, 930, 870.7 by Busemann's count in the Handbook for Experimental Physics (reference 5). The subsequent table contains the Mach numbers $M^* = \frac{u_1}{a^*}$ or $M = \frac{u_1}{a_1}$ and the Mach angle referred to the critical and local sonic velocity for these pressure factors. The ratio of the specific heats $\kappa = \frac{c_p}{c_v}$ is 1.405. The Mach numbers are a little more accurate than in the handbook. The bracketed pressure figure 999.9915 corresponds to a shock polar near the critical velocity at which equation (7) was integrated by the Busemann approximation method.

TABLE I

p-factor	$M^* = \frac{u_1}{a^*}$	$M = \frac{u_1}{a_1}$	Mach angle	$\Delta\gamma$ (deg)	Figure no.
(999.9915)	1.04106	1.050	79° 13' 43"	*	*
996	1.1714	1.2182	55° 10' 33"	4	10
992	1.2763	1.3663	47° 2' 46"	5	11
988	1.3662	1.5045	41° 39' 26"	5	12
984	1.4472	1.6403	37° 33' 42"	6	13
980	1.5221	1.7775	34° 14' 9"	6	14
976	1.5922	1.91795	31° 25' 31"	5	15
972	1.6592	2.0636	28° 59' 7"	7	16
968	1.7206	2.2157	26° 49' 43"	6	17
964	1.7798	2.3760	24° 53' 22"	7	18
956	1.8893	2.7278	21° 30' 20"	8	19
945	2.0223	3.3051	17° 36' 42"	8	20
930	2.1729	4.3776	13° 12' 19"	8	21
870.7	2.4369	∞	0°	9	22

Figures 10 to 22 represent the shock polars, meridian lines and apple curves for the several Mach numbers. (The number of the figure is given in the last column of table I.) The starting points for the meridian curves on the shock polars were so chosen that the plotted chords of the shock polars have constant difference of angle, $\Delta\gamma$ (second to the last column, table I) which amounts to 4° to 9° depending upon the Mach number. For the related cone flows it implies that at the curve Mach number the half included angles of the chosen compressibility cone form a decreasing arithmetical sequence from 90° on. The lower limit is formed by the Mach number

which, however, does not, in general, belong to the sequence. The end points of the meridian lines fix the included angle of the cone in the stream. They naturally form no simple sequence any more. The five lines plotted between shock polars and apple curve link the points of the individual meridian curves in which the difference between slope of normals and direction of speed is constant. With the notation of figure 7 they are the curves $\varphi' - \psi' = \text{Constant}$. The value of the constants is noted at the individual lines, the numerals indicate degrees, without it having been written in the figure. The direction of the normals (φ') can be computed for the points marked by the thin lines on a meridian line from the fairly accurately readable speed direction (ψ'). The reading of φ' from the figure is, in general, not quite so accurate. So for a good interpolation it is advisable to plot the relationship between ψ' and φ' in a right angled system of axis from the marked points, which then also gives, aside from the end points of the meridian line where $\varphi' = \psi' = \beta_1$ their starting point on the shock polars, where the direction of the normals is at right angles to the plotted chord. For the meridian curves arising near the axis in the subsonic range the first apple curves carry only the points, the thin lines are omitted. The end points of the meridian lines further carry the ratio of the tank pressure before and after the compressibility shock, which naturally is already established by the point u_2, v_2 on the shock polar. Moreover, the circle of the critical velocity $\sqrt{u^2 + v^2} = a^*$ is indicated by dotted lines in each figure.

The family of apple curves is represented in figure 23. The lower part gives the shock polar for each apple. The innermost dotted apple is obtained by approximation near the critical velocity and corresponds to the bracketed digits in table I. The thin system of curves permits a rough orientation of the points of the shock polars and apple curves given by the meridian curves. The exact relation is seen from figure 24(a), where the cone angle 2β is plotted against the included angle 2γ of the compressibility cone for the individual shock polars. Figure 24(b) shows as contrast the corresponding relation in the two-dimensional case between wedge angle 2β and the angle of the compressibility shock with respect to the flow direction 2γ. The aforementioned system of curves in figure 23 contains as first set the curves of equal entropy, that is, of fixed tank pressure ratio at the compressibility shock p_0'/p_0 (formula (6)), as exemplified by $\frac{p_0'}{p_0} = 0.99$, 0.9, and 0.7. The piece of the u-axis $1 \leq \frac{u_1}{a^*} \leq \sqrt{\frac{\kappa + 1}{\kappa - 1}}$

corresponds to the curve $\frac{p_o'}{p_o} = 1$. At the border of the diagram, the shock polar and apple curve for maximum velocity $\frac{u_1}{a^*} = \sqrt{\frac{\kappa + 1}{\kappa - 1}}$, $\frac{p_o'}{p_o} = 0$. As second set the straight lines u_2 = Constant were chosen. By equation (5) the pressure rise $p_2 - p_1$ at shock referred to dynamic pressure $\frac{1}{2}\rho_1 u_1^2$ is constant on the lines u_2 = Constant. The subsequent adiabatic pressure rise in the conical field after the shock up to pressure p_3 at the cone envelope is obtainable from the gas states u_2, v_2 and u_3, v_3 by adiabatic compression of p_2 by the formula

$$\frac{p_3 - p_1}{\frac{1}{2}\rho_1 u_1^2} = \frac{p_2 - p_1}{\frac{1}{2}\rho_1 u_1^2} \frac{\left(\frac{\frac{\kappa+1}{2} - \frac{\kappa-1}{2}\frac{u_3^2 + v_3^2}{a^{*2}}}{\frac{\kappa+1}{2} - \frac{\kappa-1}{2}\frac{u_1^2}{a^{*2}}}\right)^{\frac{\kappa}{\kappa-1}} \frac{p_o'}{p_o} - 1}{\left(\frac{\frac{\kappa+1}{2} - \frac{\kappa-1}{2}\frac{u_2^2 + v_2^2}{a^{*2}}}{\frac{\kappa+1}{2} - \frac{\kappa-1}{2}\frac{u_1^2}{a^{*2}}}\right)^{\frac{\kappa}{\kappa-1}} \frac{p_o'}{p_o} - 1}$$

Figure 25(a) shows the pressure ratio $\frac{p_3 - p_1}{\frac{1}{2}\rho_1 u_1^2}$ plotted against cone angle for the several apple curves, that is, airspeeds. Figure 25(b) represents the two-dimensional case of $\frac{p_2 - p_1}{\frac{1}{2}\rho_1 u_1^2}$ against wedge angle.

As in the plane, there are, in general, two flows for every possible cone angle at fixed Mach number. On sufficiently small cone angles one solution is subsonic, the other, supersonic, the latter occurring in practice. The range in which both are subsonic is greater in this instance than in the two-dimensional case. Here all points of the shock polar could be realized by considering a shock wave separated from the body. This is inapplicable here

because there is no conical field in the vicinity of an arbitrary point of the shock wave. Hence, it remains an open question which range of the apple curves and pressure curves is of practical importance. The supersonic range should be assured. A study on slightly curved conical surfaces analogous to Crocco's investigation for the wedge is not yet available.

The limit of the cone angle following from the apple curves for a specific Mach number is shown in figure 26, along with the maximum wedge angle. The angle zone 1 is characterized by the fact that for these angles wedge, as well as cone, flows exist, where the shock surface adheres to the edge or tip. The second range includes the angles where the knife edges are worse, because the shock surface has become detached, but the tips are still useful. In the third range the shock surfaces for both the wedge and the cone lie upstream from the body. Figures 27(a) and 28(a) are modifications of figures 24(a) and 25(a); the Mach number is consistently marked off on the axis of abscissa. The axis of the ordinate contains the size of the compressibility shock and pressure ratio. The individual curves correspond to cones of fixed included angles. The limiting curve $\beta = 0$ shown as dash and dot line (-.-.-) in figure 28(a) indicates the pressure jump before a blunt obstacle. If the adiabatic compression up to the stagnation at the body is also taken into account, it affords the plotted pitot pressure (Prandtl-Rayleigh).

Figures 27(b) and 28(b) represent the two-dimensional case.

For several cone angles (supersonic range after the shock) the pressure calculation by (11a) gives the simple approximation formula:

$$\frac{p_3 - p_1}{\frac{1}{2}\rho_1 u_1^2} = 2\beta^2 \ln \frac{2}{\beta\sqrt{M^2 - 1}}$$

at which the logarithmic singularity and Mach relationship is correctly defined, but the numerical factor 2 behind the logarithm is likely to be uncertain in certain circumstances.

In conclusion, the integration of equation (7) for the apple curve in vicinity of the initial velocity is stressed. As demonstrated by Busemann, a suitable substitution makes it possible to range equation (7) into a differential equation independent of the Mach number M and the specific ratio κ. The same substitution frees the shock polar and hence the initial conditions of the meridian lines from M and κ. They are employed only for the determination of the end point of the meridian lines.

Figure 29 indicates the results of the integration in the coordinates x and y for the meridian lines independent of M and κ, which are related with u and v through

$$y = \frac{\kappa + 1}{2} \frac{1}{(M - 1)^{3/2}} \frac{v}{a^*} \qquad x = \frac{\kappa + 1}{2} \frac{u - a^*}{a^*} \frac{1}{M - 1}$$

The initial abscissa on the shock polars is written at the meridian curves. The subsequent meridian lines (not shown) can be replaced by curves $y = ae^{bx}$. The related constants a and b can be taken from table II.

TABLE II

x_2	a	b
-0.95	0.00755	-3.59
-.9	.0298	-2.66
-.5	.324	-1.48
0	.763	-1.37
.25	1.02	-1.46
.5	1.39	-1.68
.75	2.28	-2.30
.9	6.03	-3.59
.97	75.4	-6.65

The end point of the meridian lines for a given M and κ follows from the equation

$$y_3 y_3' = -\frac{2}{\kappa + 1} \frac{1}{(M - 1)^2} - \frac{x}{M - 1}$$

The dash denotes the derivation with respect to x.

Translated by J. Vanier
National Advisory Committee
for Aeronautics

REFERENCES

1. Meyer, Th.: Über zweidimensionale Bewegungsvorgänge in einem Gas, das mit Überschallgeschwindigkeit strömt. Dissert. Göttingen, Forschungsarbeiten auf dem Gebiete des Ingenieurwesens, VDI Heft 62, 1908.

2. Busemann, A: Drücke auf kegelförmige Spitzen bei Bewegung mit Überschallgeschwindigkeit. Z. angew. Math. Mech. Bd. 9, 1929, p. 496.

   Busemann, A.: Die achsensymmetrische kegelige Überschallströmung. Luftf.-Forschg. Bd. 19, 1942, pp. 137-144.

3. Busemann, A.: Aerodynamischer Auftrieb bei Überschallgeschwindigkeit Convegno di sci. fis. mat. nat., Roma 1935, p. 345 und Luftf.-Forschg. Bd. 12, 1935, p. 217.

4. Crocco, L.: Singolarità della corrente gassosa iperacustica nell' intorno di una prora a diedro. Aerotecnica Bd. 17, 1937, p. 519.

5. Busemann, A.: Gasdynamik in Wien-Harms, Handbuch der Experimentalphysik Bd. IV, 1, 1931, p. 426.

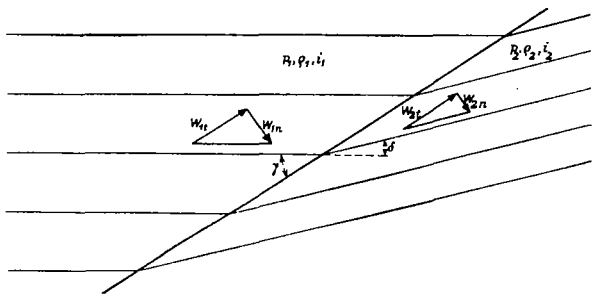

Figure 1. Conditions at the two-dimensional compressibility shock.

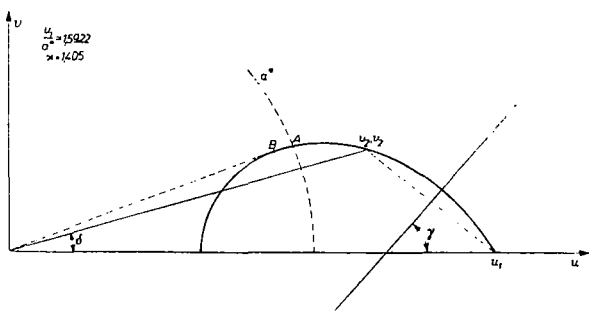

Figure 2. Shock polars

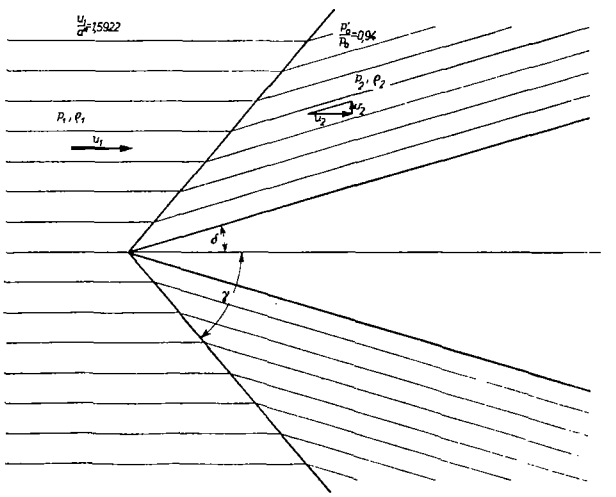

Figure 3.- Wedge in supersonic flow (κ = 1.405); the related shock polar is shown in figure 2.

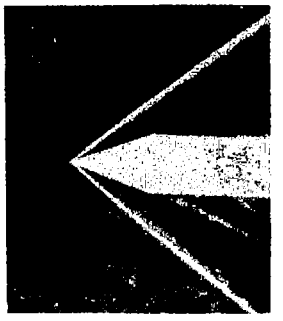

Figure 4a.- Schlieren photograph of wedge for adhering compressibility shock.

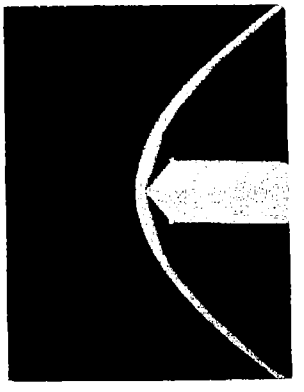

Figure 4b.- Schlieren photograph of wedge for separated compressibility shock.

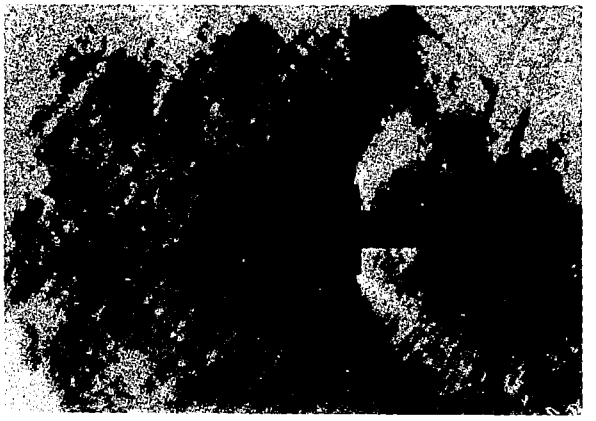

Figure 5a.- Schlieren photograph of cone for adhering compressibility cone.

Figure 5b.- Schlieren photograph of cone for separated compressibility cone.

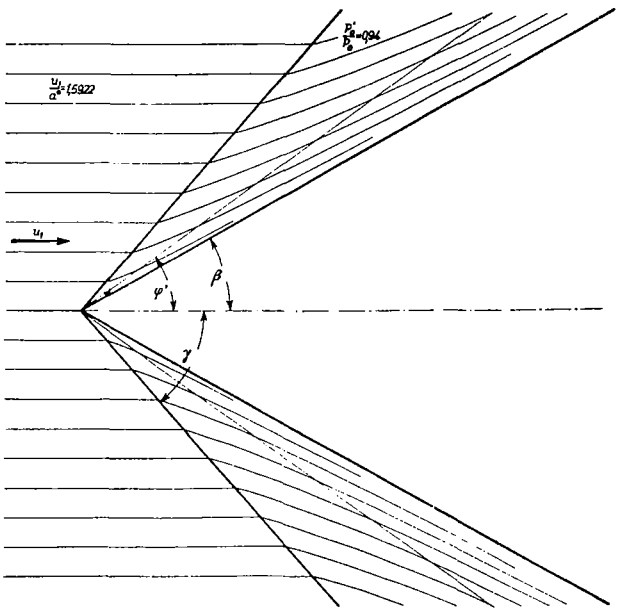

Figure 6.- Supersonic flow around a cone in axial section (related hodograph shown in figure 7).

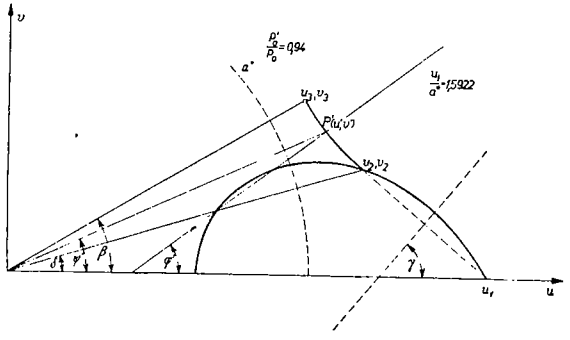

Figure 7. Hodograph of an axial section of a cone.

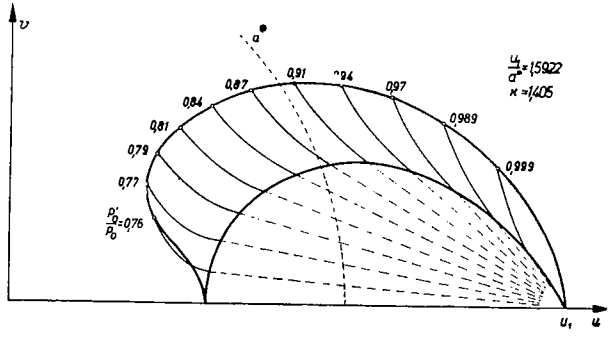

Figure 8. Construction of the meridian curve.

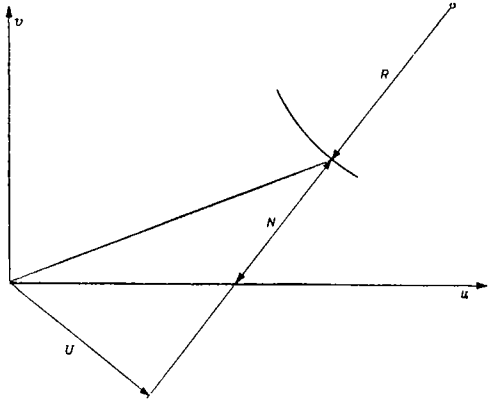

Figure 9. Apple curve with meridian lines and shock polar.

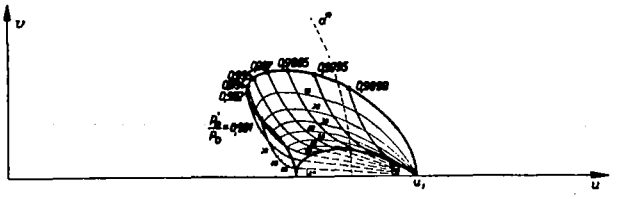

Figure 10. P-factor 996, $\frac{u_1}{a_*} = 1{,}1714$, $\frac{u_1}{a_1} = 1{,}2182$.

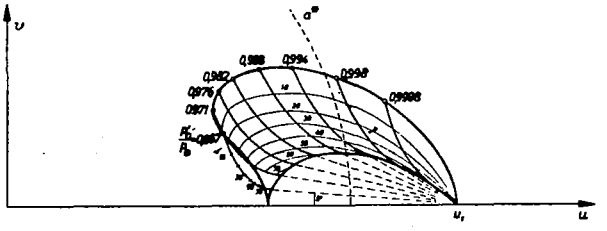

Figure 11. P-factor 992, $\frac{u_1}{a^*} = 1{,}2763$, $\frac{u_1}{a_1} = 1{,}3663$.

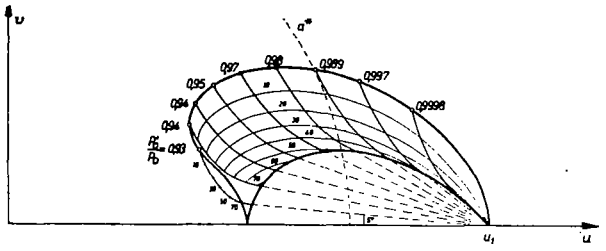

Figure 12. P-factor 988, $\frac{u_1}{a^*} = 1{,}3662$, $\frac{u_1}{a_1} = 1{,}5045$.

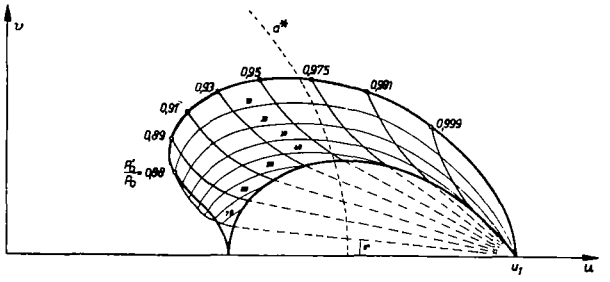

Figure 13. P-factor 984, $\frac{u_1}{a^*} = 1{,}4472$, $\frac{u_1}{a_1} = 1{,}6403$.

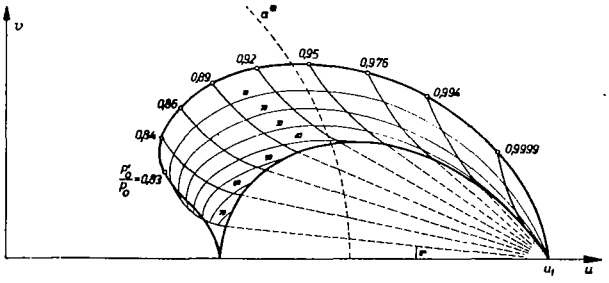

Figure 14. P-factor 980, $\frac{u_1}{a^*} = 1{,}5221$, $\frac{u_1}{a_1} = 1{,}7775$.

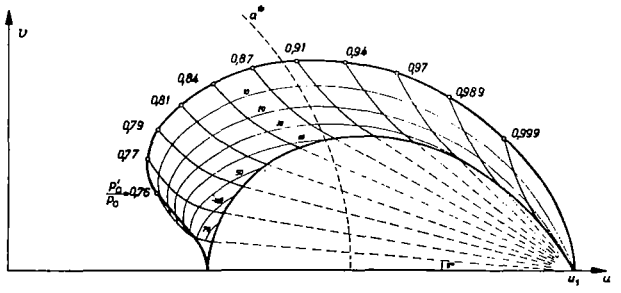

Figure 15. P-factor 976, $\frac{u_1}{a^*} = 1{,}5922$, $\frac{u_1}{a_1} = 1{,}91795$.

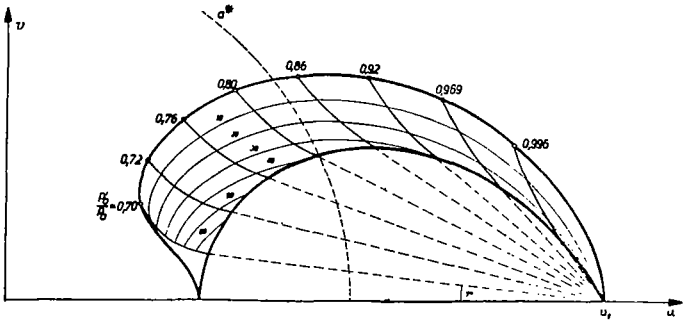

Figure 16. P-factor 972, $\frac{u_1}{a^*} = 1{,}6582$, $\frac{u_1}{a_1} = 2{,}0636$.

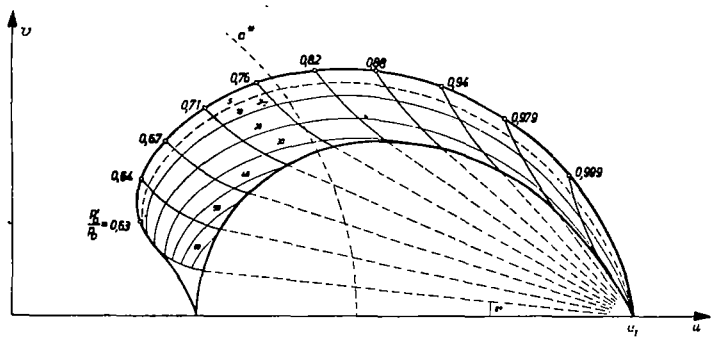

Figure 17. P-factor 968, $\frac{u_1}{a^*} = 1{,}7206$, $\frac{u_1}{a_1} = 2{,}2157$.

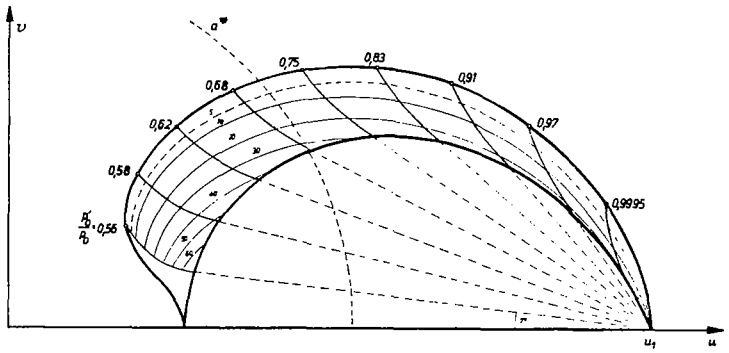

Figure 18. P-factor 964, $\frac{u_1}{a^*} = 1{,}7798$, $\frac{u_1}{a_1} = 2{,}3760$.

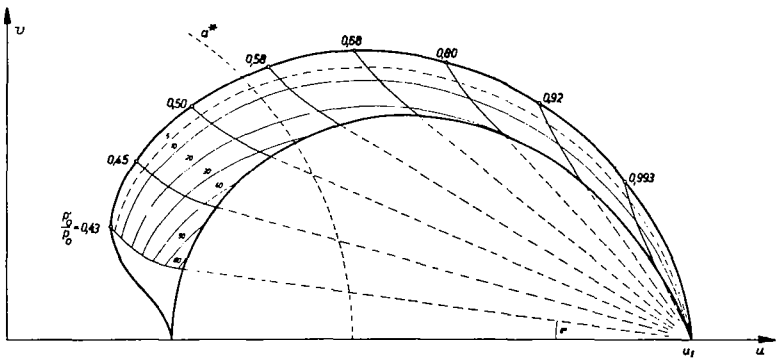

Figure 19. P-factor 956, $\frac{u_1}{a^*} = 1{,}8893$, $\frac{u_1}{a_1} = 2{,}7278$.

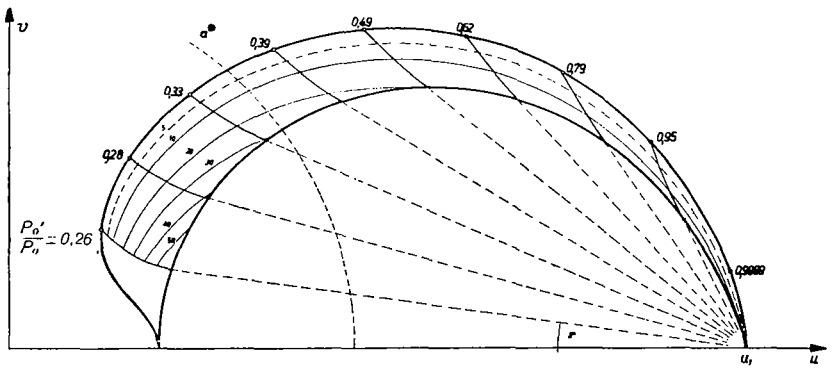

Figure 20. P-factor 945, $\frac{u_1}{a^*} = 2{,}0223$, $\frac{u_1}{a_1} = 3{,}2051$.

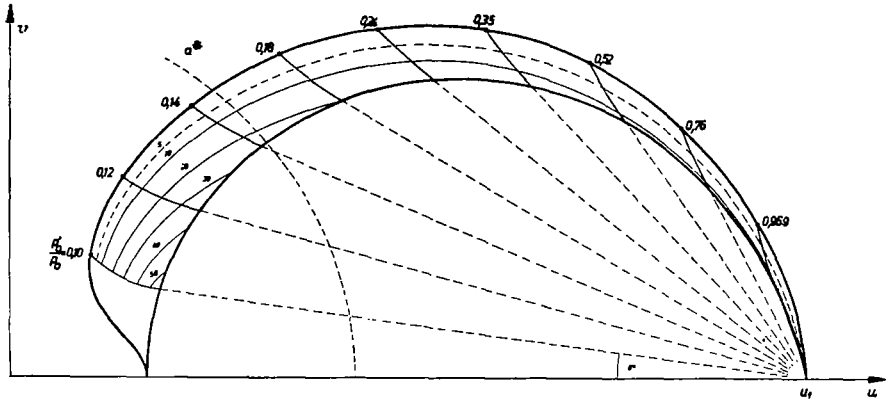

Figure 21. P-factor 930, $\frac{u_1}{a^*} = 2{,}1729$, $\frac{u_1}{a_1} = 4{,}3776$.

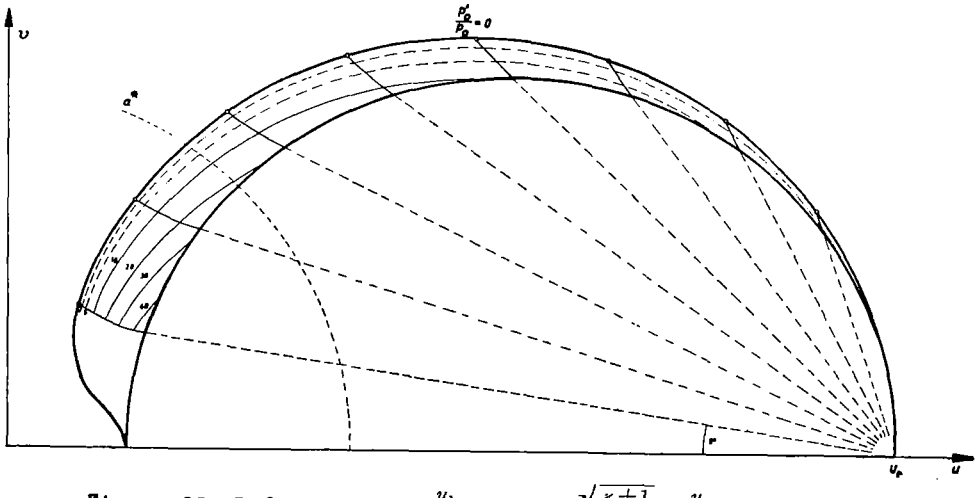

Figure 22. P-factor 870,7, $\frac{u_1}{a^*} = 2{,}4369 = \sqrt{\frac{\varkappa+1}{\varkappa-1}}$, $\frac{u_1}{a_1} = \infty$.

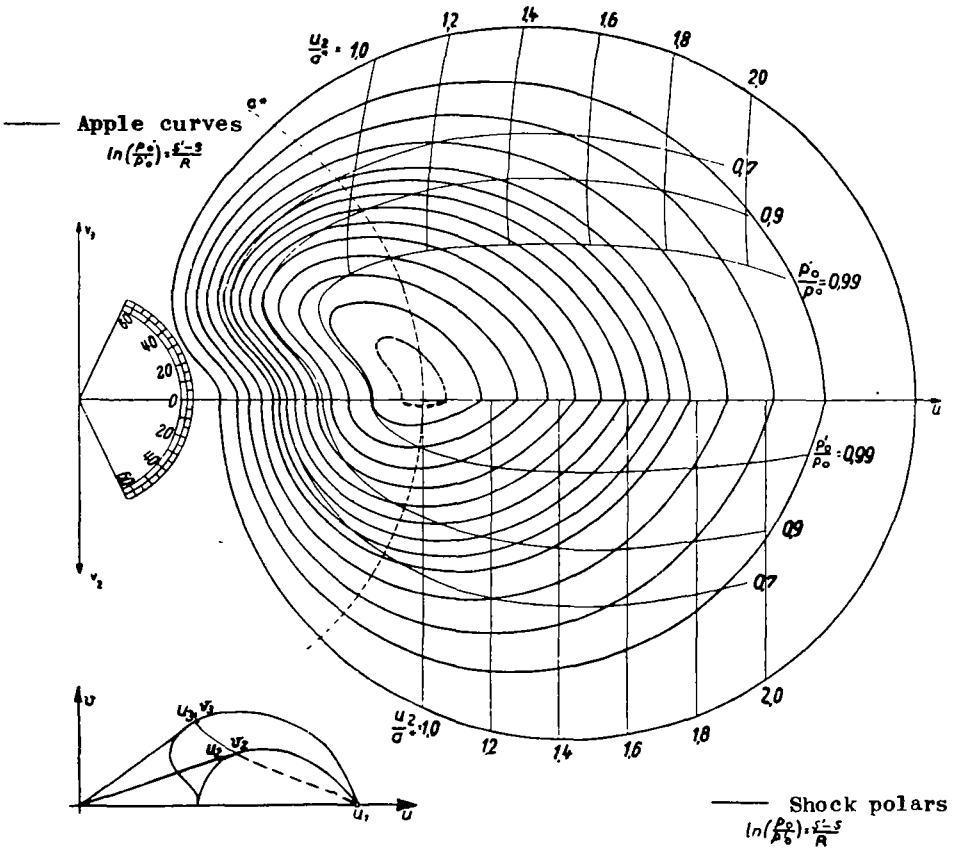

Figure 23. Family of apple curves and shock polars.

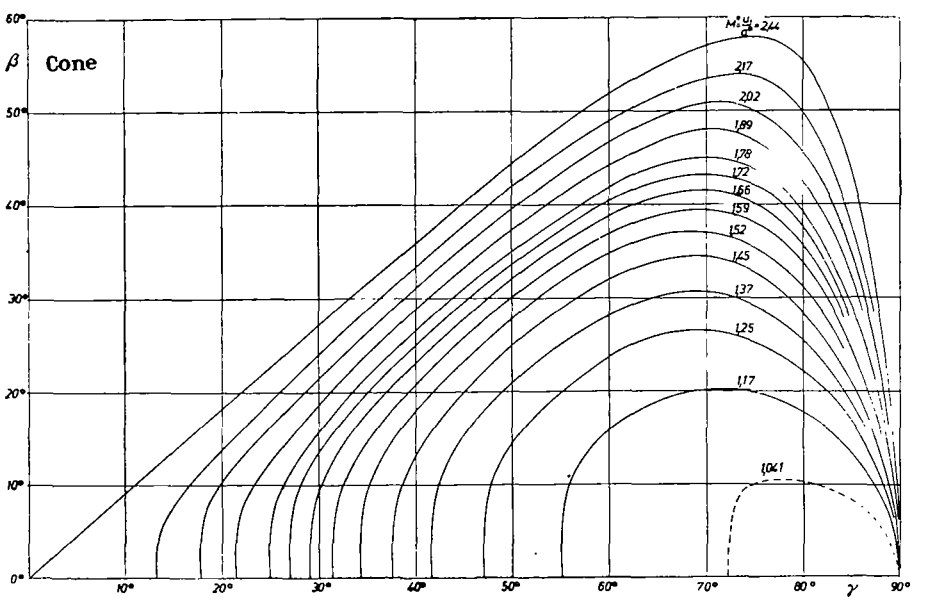

Figure 24a. Relationship between half the cone angle β and half included angle γ of the compressibility shock at different air speeds.

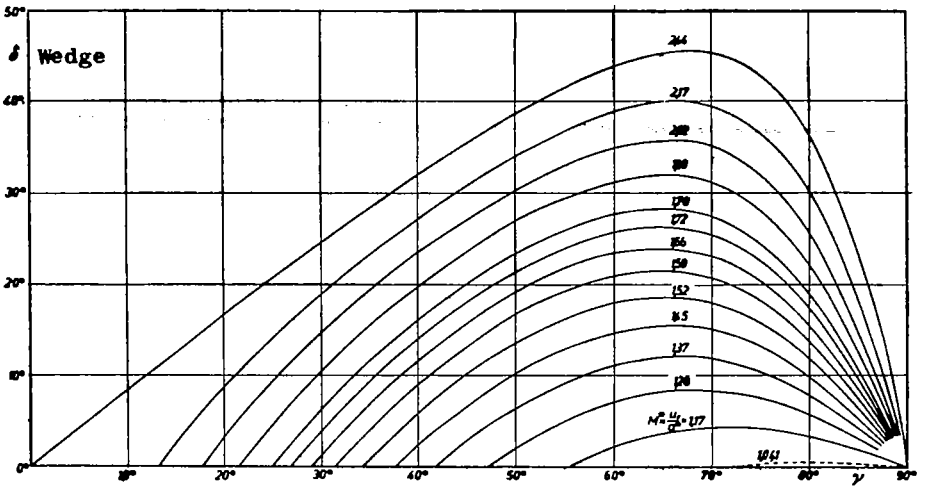

Figure 24b. Relationship between half wedge angle δ and angle of slope between compressibility shock and flow velocity at different air speeds.

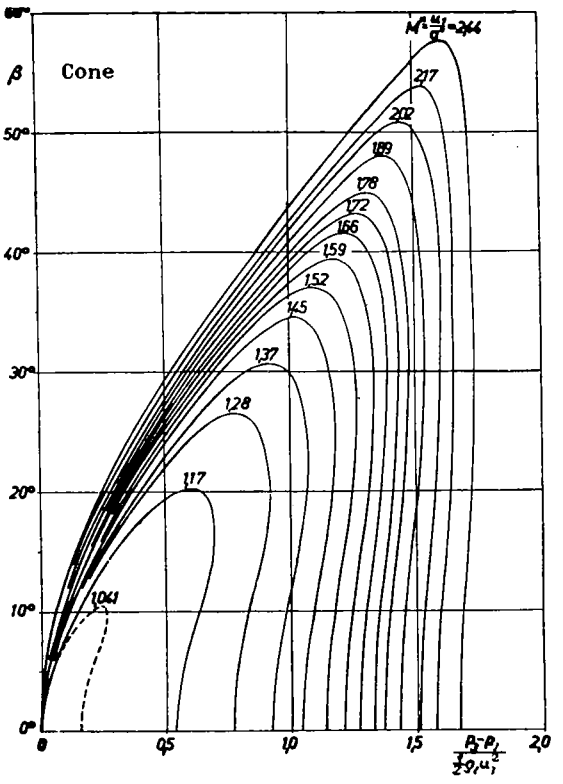

Figure 25a.- Pressure on cone surface plotted against $\frac{1}{2}$ cone angle β for different air speeds. (p_3 pressure at cone envelope, p_1 pressure of flow, $\frac{1}{2}\rho_1 u_1^2$ dynamic pressure.)

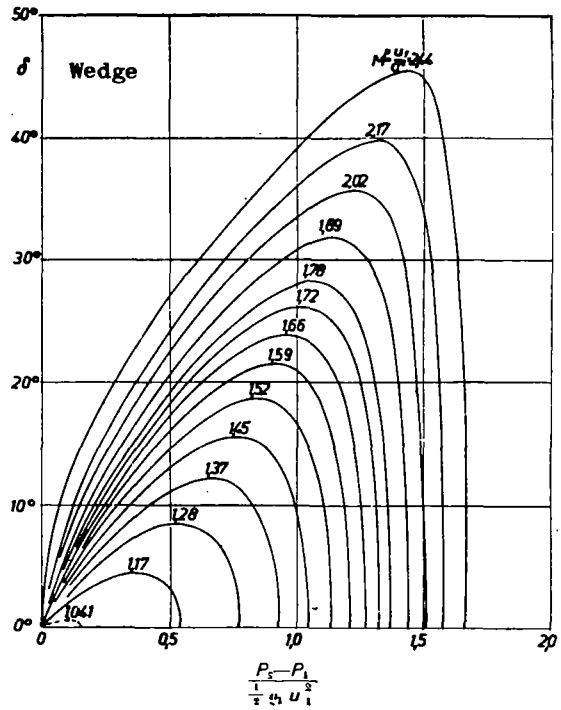

Figure 25b. Pressure jump $p_2 - p_1$ at compressibility shock referred to dynamic pressure in relation to $\frac{1}{2}$ wedge angle δ for different air speeds.

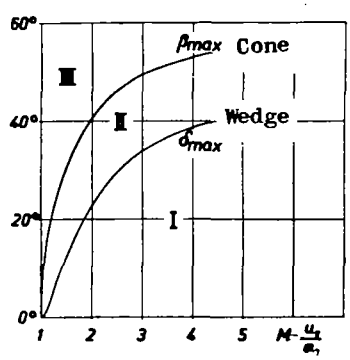

Figure 26. Limiting value of the half cone angle and wedge angle for adhering compressibility shock plotted against Mach number.

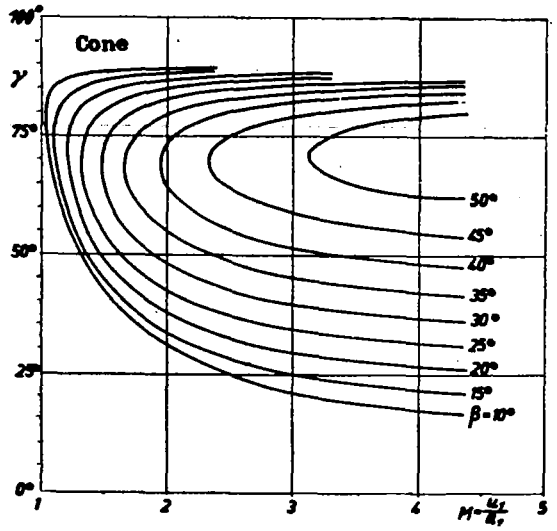

Figure 27a. Half included angle of compressibility shock against the Mach number for different cone angles 2 β .

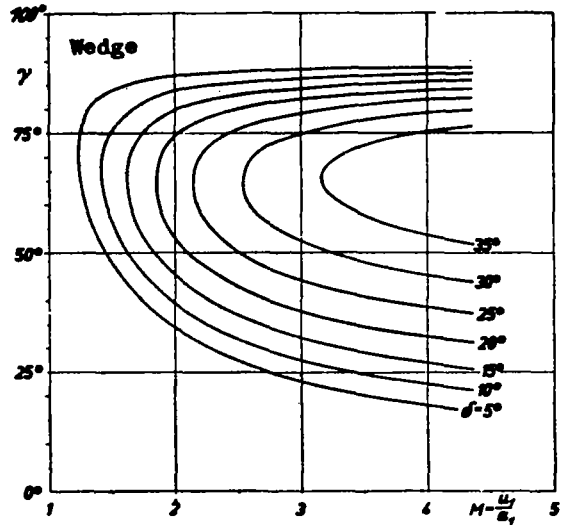

Figure 27b. Slope γ of compressibility shock against flow for different wedge angles 2 δ as function of the Mach - number.

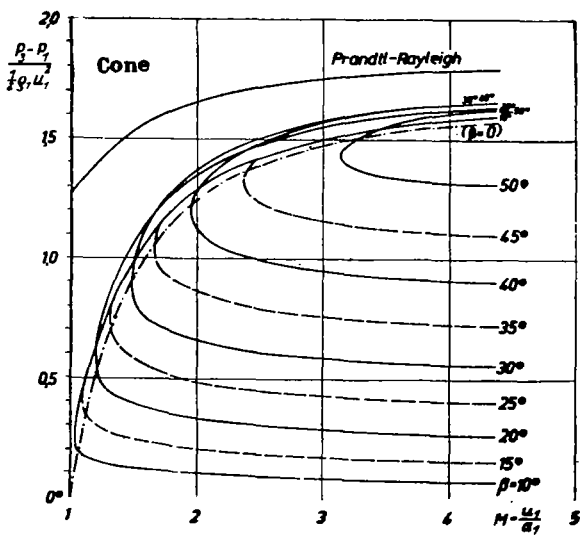

Figure 28a.- Pressure on cone surface in relation to Mach number for different included angles 2 β (p_3 pressure at cone envelope, p_1 pressure of flow, $\frac{1}{2}\rho_1 u_1^2$ dynamic pressure).

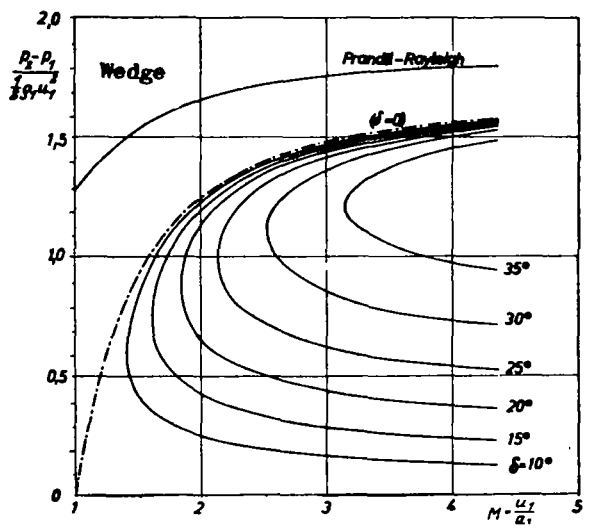

Figure 28b. Pressure jump at compression shock referred to dynamic pressure for several wedge angles 2 δ against the Mach number.

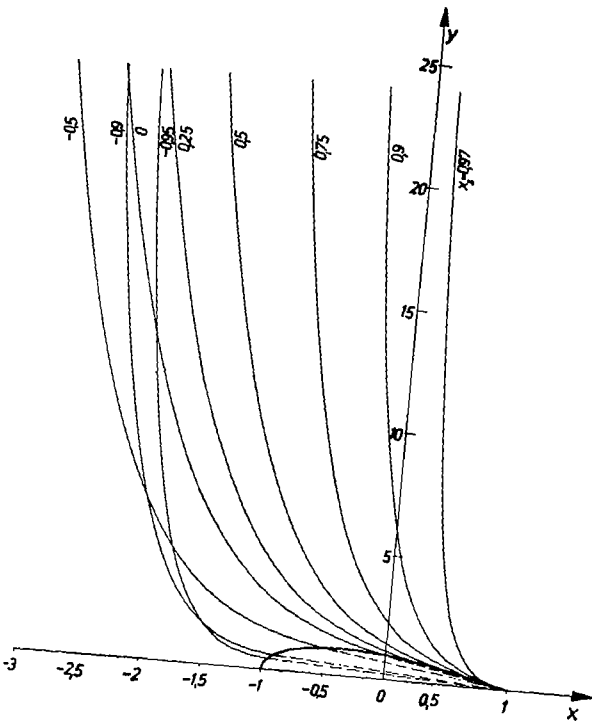

Figure 29. Approximate solution for the vicinity of the critical speed.

NASA Technical Library
3 1176 01437 4616